AGU PUBLICATIONS

Geophysical Research Letters

RESEARCH LETTER
10.1002/2014GL059963

Key Points:
- Diapycnal mixing decreases near linearly away from the bottom
- Expanding AABW cell thus experience reduced mixing during the glacial
- Near-linear vertical mixing profiles in models could initiate a glacial cycle

Correspondence to:
A. M. De Boer,
agatha.deboer@geo.su.se

Citation:
De Boer, A. M., and A. M. C. Hogg (2014), Control of the glacial carbon budget by topographically induced mixing, *Geophys. Res. Lett.*, *41*, 4277–4284, doi:10.1002/2014GL059963.

Received 20 MAR 2014
Accepted 28 MAY 2014
Accepted article online 2 JUN 2014
Published online 18 JUN 2014

Control of the glacial carbon budget by topographically induced mixing

Agatha M. De Boer[1] and Andrew McC. Hogg[2]

[1]Bolin Centre for Climate Research and Department of Geological Sciences, Stockholm University, Stockholm, Sweden, [2]Research School of Earth Sciences and ARC Centre of Excellence for Climate System Science, Australian National University, Canberra, ACT, Australia

Abstract Evidence for the oceanic uptake of atmospheric CO_2 during glaciations suggests that there was less production of southern origin deep water but, paradoxically, a larger volume of southern origin water than today. Here we demonstrate, using a theoretical box model, that the inverse relationship between volume and production rate of this water mass can be explained by invoking mixing rates in the deep ocean that are proportional to topographic outcropping area scaled with ocean floor slope. Furthermore, we show that the resulting profile, of a near-linear decrease in mixing intensity away from the bottom, generates a positive feedback on CO_2 uptake that can initiate a glacial cycle. The results point to the importance of using topography-dependent mixing when studying the large-scale ocean circulation, especially in the paleo-intercomparison models that have failed to produce the weaker and more voluminous bottom water of the Last Glacial Maximum.

1. Introduction

The atmospheric CO_2 concentration during the Last Glacial Maximum (LGM) was about 100 ppm (parts per million) less than in preindustrial times. Most of this difference is thought to be a result of a more efficient oceanic biological pump [*Sigman and Boyle*, 2000; *Sigman et al*., 2010]. The efficiency of the biological pump is directly related to the deep ocean ratio of regenerated nutrients (derived from organic fallout) to preformed nutrients (that are advected downward through bottom water formation) [*Ito and Follows*, 2005; *Toggweiler et al*., 2006; *de Boer et al*., 2010b]. Antarctic Bottom Water (AABW) is the main source of preformed nutrients to the abyssal ocean so that a decrease in production rate of this water mass compared with North Atlantic Deep Water is required to explain the drawdown of carbon to the deep ocean [*Toggweiler et al*., 2006; *de Boer et al*., 2010b]. However, chemical proxy evidence indicates that the volume fraction of deep water formed in the Southern Ocean relative to that formed in the North Atlantic was greater during the LGM than today [*Lynch Stieglitz et al*., 1996; *Curry and Oppo*, 2005; *Skinner*, 2009; *Lund et al*., 2011; *Adkins*, 2013]. Thus, a complete theory for glacial atmospheric CO_2 and water mass distribution must account for larger volumes of southern origin water produced at a slower rate. The problem is that processes that increase the volume of southern origin water (such as increased cooling or brine rejection) often also increase its rate of production.

The strength of the AABW cell, which describes the rate of AABW formation, is thought to be partly controlled by diapycnal mixing [*Kamenkovich and Goodman*, 2000; *Nikurashin and Ferrari*, 2013]. Therefore, reduced overturning of southern origin water during the glacial implies reduced mixing between this water mass and the northern origin deep water above it. This reduced mixing during the last glacial has been attributed to two mechanisms. In the first mechanism, saltier and thus denser southern origin water enhances the deep stratification, thereby inhibiting turbulent mixing with the overlying water [*Watson and Garabato*, 2006; *Bouttes et al*., 2010, 2011]. In the second mechanism, there is less mixing across the interface between the southern and northern origin water masses because its shallower depth is farther away from the bottom topography [*Lund et al*., 2011; *Adkins*, 2013]. The current study relates to this second mechanism which relies on the well-established link between diapycnal mixing and topography; enhanced diapycnal mixing decays vertically away from topography [*Saenko et al*., 2012] and may be driven by tidal [*Ledwell et al*., 2000] or mesoscale eddy [*Dewar and Hogg*, 2010; *Nikurashin and Ferrari*, 2010; *Zhai et al*., 2010] interactions with the topography.

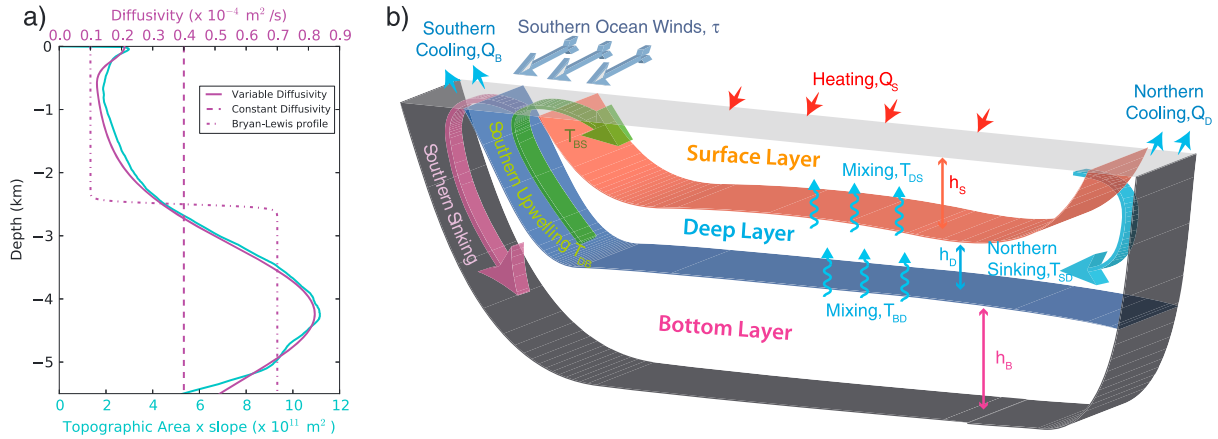

Figure 1. (a) Total area of the ocean floor that lies below and within 100 m of each depth scaled with the slope (cyan) and the diffusivity profile used in the VarD (solid magenta), ConD (dashed magenta), and Bryan-Lewis (dash-dotted magenta) simulations. (b) Idealized model that estimates water mass formation rates and the thickness of each of the three layers as a function of prescribed Southern Ocean wind stress and surface buoyancy forcing. Buoyancy is fluxed into the ocean at the tropics and out of the ocean at both polar regions.

2. Role of the Vertical Diffusivity Profile

Here we introduce a topography-dependent mixing profile (Figure 1a) into a three-layer box model for the ocean overturning circulation, based on *Shakespeare and Hogg* [2012]. We use this model to investigate the role that this mixing profile plays in the progression toward less AABW production and a large AABW cell during the last glacial. The model follows a history of idealized models [*Gnanadesikan*, 1999] which have been used to understand the fundamentals of the ocean circulation. It consists of a surface, deep, and bottom water layer whose thicknesses are represented by h_i where i is S, D, and B for the surface, deep, and bottom layers respectively (Figure 1b). Each layer outcrops and is subjected to a buoyancy forcing Q_i. The volume transports (or transformation rates) from layer i to j are represented as T_{ij}. North Atlantic Deep Water formation is diagnosed as the rate of transformation from the surface to deep layer (T_{SD}), while the rate of AABW formation is represented by T_{BD} which closes the bottom water cell. See Appendix A for a detailed model description and the preindustrial forcing values of the reference state (Figure 2, circles).

The evolution toward a glacial ocean stratification is simulated using two perturbations to the surface forcing. In the first, the Southern Ocean is cooled or salinified by increasing the surface buoyancy flux from the Southern Ocean (i.e., Q_B, with the constraint that $Q_S = Q_B + Q_D$), and in the second, the Southern Ocean wind stress (τ) is decreased. We compare the response of the ocean to changes in Southern Ocean surface buoyancy forcing (Figure 2a) and wind forcing (Figure 2b) in a model with a constant vertical diffusivity (ConD, of 4×10^{-5} m^2/s) and a topography-dependent vertical diffusivity profile (VarD, see magenta lines in Figure 1a). The latter diffusivity profile is based on the sum of the area of ocean floor within 100 m of a given depth and derived from the 2 min *Smith and Sandwell* [1997] topography data version 8.2 between 72°S and 72°N. Each grid point area is weighted by the slope of the floor at that location to reflect observations that mixing is enhanced about rough topography [*Polzin et al.*, 1997]. The resulting profile decreases near linearly with depth from 4 km upward to about 2 km (Figure 1a, cyan line).

For all the glacial forcing simulations the bottom layer becomes thicker and denser. However, the bottom water formation rate response of the simulations depends critically on the vertical diffusivity parameterization. For the ConD runs (Figure 2, dashed lines) the bottom water formation increases in concert with the bottom layer thickness, but for the VarD runs (Figure 2, solid lines) the formation rate decreases with increasing layer thickness. In the VarD runs, the thickening of the bottom layer pushes the interface of the bottom layer up into a region with weaker mixing and thereby reduces the rate of bottom water formation. Note that we have also created and tested a profile that is solely dependent on the area of ocean floor at a certain depth (i.e., not weighted by the slope of the floor). The resulting profile (not shown) is qualitatively similar (peaking at ~4 km and near-linearly decreasing until about ~2 km) with only slightly larger differences between deep and surface values. We have further repeated the analysis for topography horizontal resolutions of 0.1 and 0.5°

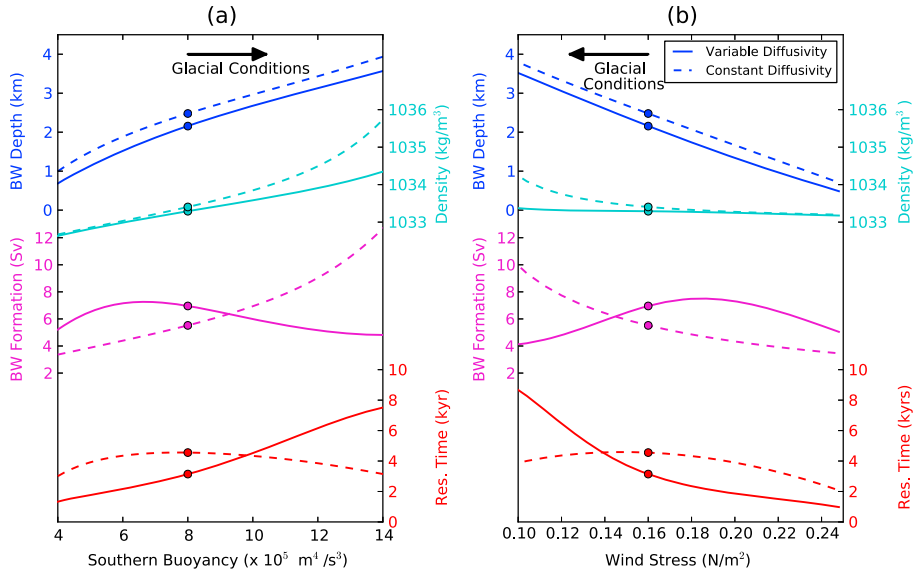

Figure 2. Sensitivity of the model to increasing (a) southern buoyancy extraction and (b) wind stress. The response of the interface height is represented here as the inverse bottom water (BW) depth or thickness (dark blue). Also shown is the response of the bottom layer density (cyan), BW production (magenta), and the bottom layer residence time (red). Solid lines show the VarD case while dashed lines show the results for ConD. Solid circles show reference state solution.

and found no difference in the basic profile or our conclusions. Interestingly, this suggests that most of the ocean floor is rough and it is primarily the area of ocean floor that determines how much mixing occurs at a certain depth.

In the paleorecord, low values of $\delta^{13}C$ and $\Delta^{14}C$ in the deep ocean during the glacial are suggestive of a reduced bottom water formation rate and a long residence time [*Hodell et al*., 2003; *Toggweiler et al*., 2006; *Burke and Robinson*, 2012]. In our model the bottom residence time is given by the volume of the bottom water divided by its production rate. Even though the decreases in the AABW formation rates in the VarD glacial simulations are small, they increase the residence times by several thousands of years (Figure 2, red lines). This is because, in a well-mixed volume, only a small change in overturning rate is needed to produce a large change in the residence time [*de Boer et al*., 2008]. The old ages produced in the VarD runs are not seen for the ConD cases because in the ConD runs the increase in the volume of bottom water that is ventilated is compensated by an increase in the bottom water formation rate.

Lund et al. [2011] estimate the ratio of the abyssal overturning circulation to vertical diffusivity in the deep ocean to be approximately 8 times larger during the LGM, primarily due to the expansion of the areas covered by bottom water in the Atlantic. In our model, this quantity is written (using the final equation in the Appendix A) as $T_{BD}/K_v = A/h_D$. While the area, A, does not vary in our model, the middepth layer become thinner (h_D decreases) such that this parameter doubles in both glacial scenarios. Thus, we find qualitative agreement with existing proxy records.

The glacial integrations presented thus far apply a fixed surface forcing field to simulate the reduced bottom water formation and thicker bottom water mass. This bottom water would store more dissolved inorganic carbon that result from accumulation and remineralization of sinking biological material. In reality, we envision that the initial surface cooling and brine rejection (or reduction in winds) would be weak but that the consequent reduction in atmospheric CO_2 would lead to further surface buoyancy loss (or weakening winds) in a positive feedback loop. We simulate such a glacial inception by running transient simulations in which Southern Ocean surface buoyancy loss is assumed to be linearly proportional to bottom water residence time. While this is admittedly a very crude parameterization of feedbacks in the global carbon cycle, it demonstrates the principle that such a weak positive feedback effect can generate a glacial state in a free-running model (Figure 3). Moreover, the positive feedback is only significant when variable diffusivity acts to reduce bottom water production as the layer thickens.

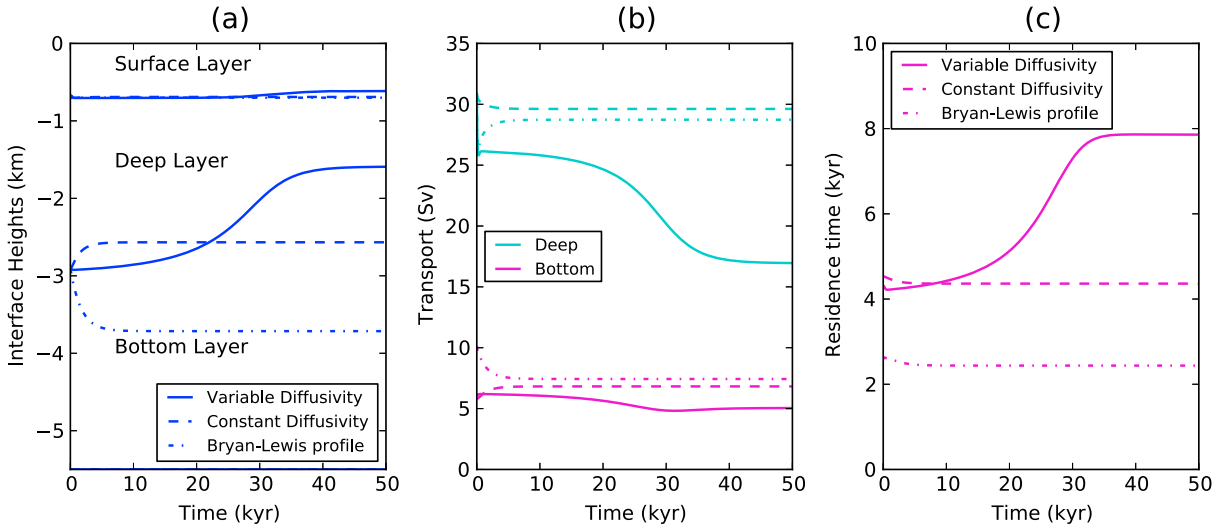

Figure 3. Transient simulation showing the evolution of (a) interface height, (b) layer transport, and (c) bottom water residence time for VarD (solid lines), ConD (dashed), and Bryan-Lewis (dash-dotted) cases in which southern buoyancy forcing is assumed to be proportional to bottom water residence time.

3. Implications for Ocean Circulation Modeling

High-resolution ocean and climate models now routinely parameterize diapycnal mixing by sophisticated tidal and/or stratification-dependent mixing schemes. However, most of the ocean models that are used to study the dynamics of the large-scale ocean circulation are run for many thousands of years and use simpler and computationally cheaper options. In such models, the intense mixing in the deep ocean is often represented by the so-called Bryan-Lewis profile [*Bryan and Lewis*, 1979]. This profile describes a tangent function that has a very low vertical diffusivity (typically $10^{-5}\,m^2/s$) in the upper layer and a higher value (typically $10^{-4}\,m^2/s$) in the lower layer. The transition between the layers is rather sharp and usually set between 1000 m and 2500 m depth. The deeper part of the ocean (below 2500 m) therefore has a constant vertical diffusivity, and the overturning rate of bottom water would not decrease as the bottom layer thickens, in the manner we suggest happens during a glacial inception. We confirm in our model that a Bryan-Lewis-type diffusivity profile (dash-dotted line in Figure 1) is not capable of initiating a glacial state through the AABW volume-mixing rate feedback (Figure 3, dash-dotted line).

Until now, it has not been trivial for climate models to simulate a weaker but more voluminous bottom water cell for the last glacial. Only one of the nine models used in the Paleoclimate Modelling Intercomparison Project versions (PMIP)1.5 and PMIP2, the Hadl2 model, generated an inverse relationship between AABW volume and production rate for the LGM [*Weber et al.*, 2007]. We test here the hypothesis that the models' failure may be related to their vertical diffusivity parameterization. Toward that purpose, we compare for all nine PMIP preindustrial simulations and their LGM equivalent the change in AABW thickness and formation rate (Figure 4). The residence time is also calculated as the AABW layer thickness divided by the formation rate (Figure 4). In seven of the models, the AABW production rate (Figure 4, blue) changed with the same sign as the thickness (Figure 4, red). In the Hadl1.5 model the AABW layer thickness did not change, and the formation rate increased. Only in the Hadl2 model did the AABW layer thickness and production rate change with an opposing sign as predicted by our simple model for a variable diffusivity that decreased near linearly away from the bottom.

The vertical diffusivity schemes used in the simulations were not mentioned in the comparison paper [*Weber et al.*, 2007] and also not in the publications that were listed as the reference for each model. Information about the schemes was therefore obtained through personal communication with the lead authors where possible. In some cases the parameters were lost, but in most cases some knowledge of the scheme and parameters used were still available. The Hadl2 and Had1.5 were the only models that used a vertical diffusivity profile that decreased linearly away from the bottom (i.e., from about $14 \times 10^{-5}\,m^2/s$ at the bottom to about $1 \times 10^{-5}\,m^2/s$ at the surface). Most of the models (i.e., CCSM, ECBilt, UVic, UTor, and ClimC) used a

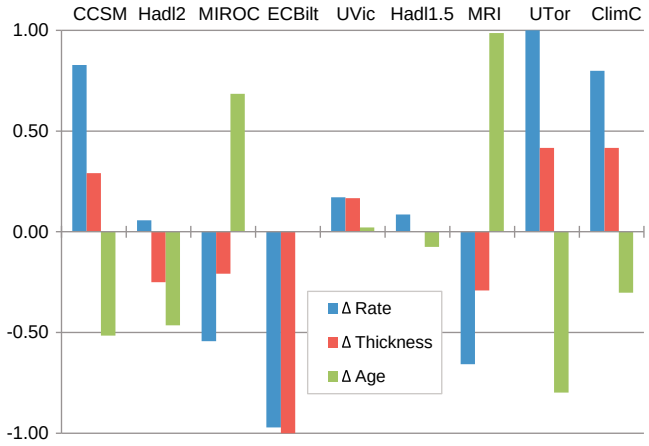

Figure 4. Difference in southern origin water formation rates, thickness, and age between the LGM and present-day simulations of five PMIP2 models (left five bars: CCSM, Hadl2, MIROC, ECBILT, and UVIC) and four PMIP1.5 models (right four bars: Hadl1.5, MRI, UTor, and ClimC). All values have been normalized by their maximum which was 2400 m for the thickness and 3.5 Sverdrup for the formation rate. Note that the age difference for the ECBilt model was set to zero because their LGM simulation had no southern origin water at all. Data are from Table 2 in *Weber et al*. [2007].

scheme with a Bryan-Lewis profile or a step change in diffusivity and these all result in near-constant high diffusivities in the deep ocean below about 2.5 km depth. The MIROC and MRI models used a version of the *Mellor and Yamada* [1982] scheme, but we have no further information about that. The lack of official documentation of the diffusivity used in these models and the absence of any mention of it when describing and analyzing the large-scale overturning circulation in the LGM simulations [*Otto-Bliesner et al*., 2007; *Weber et al*., 2007] suggest that its importance is not appreciated yet in all communities that aim to understand and model deep water formation processes.

As we saw, the only two models that produced an inverse change (or no change) between AABW cell thickness and production rate were also the only two models that had a vertical mixing profile that decrease linearly away from the bottom. There are of course many factors that influence the relative formation rates and sizes of deep water masses (such as winds, buoyancy forcing, resolution, and model components) so that even the Hadl2 model failed to produce a lower AABW production rate and thicker water mass. However, given the results here and our current improved understanding of the role of topography on mixing, there is strong motivation to improve the vertical diffusivity schemes in models used to study the large-scale overturning. A simple and computationally efficient improvement would be to include a diffusivity profile that has high diffusivity only in the layer above a geographically varying bottom. In ocean models that have a mostly flat bottom, such as idealized aqua-planet models [e.g., *De Boer et al*., 2007] or theoretical and box models, a profile that decreases linearly away from the bottom everywhere as in Figure 1a would be more appropriate than the commonly used constant diffusivity or Bryan-Lewis profile.

The role of the mixing profile in setting a realistic glacial ocean circulation can easily be tested in general circulation models of the ocean. If the topographically dependent mixing profile captures the glacial circulation in a wide suite of models, it would provide important new insight about how the distribution of mixing affects the volume and production rates of abyssal water masses. It would also provide further support for the hypothesis that southern origin bottom water during the glacial evolved to be both more voluminous and despite a lower production rate than today due to weaker upper layer mixing. On a philosophical note, the study shows how the paleorecord can inform us about the dynamics of the modern ocean and by implication how it may respond to future climate change.

Table 1. Default Parameters Used for the Preindustrial Control State

Parameter	Value
τ	$0.16\,\mathrm{N/m^2}$
Q_S	$20\times10^5\,\mathrm{m^4/s^3}$
Q_B	$8\times10^5\,\mathrm{m^4/s^3}$
Q_D	$12\times10^5\,\mathrm{m^4/s^3}$
L_x	22 000 km
ρ_0	$1030\,\mathrm{kg/m^3}$
f_{ACC}	$7\times10^{-5}\,\mathrm{s^{-1}}$
A	$3.2\times10^{14}\,\mathrm{m^2}$
K_v	$4\times10^{-5}\,\mathrm{m^2/s}$
a_{SD}	1200
$a_{e,S}$	600
$a_{e,D}$	150

Appendix A: Model Description

We have adapted the three-layer model described by *Shakespeare and Hogg* [2012] to evolve with time and to include a simple parameterization for diffusive buoyancy

fluxes (Figure 1b). The model consists of conservation of volume equations for the surface and bottom layers,

$$A\,\frac{\partial h_S}{\partial t} = T_{BS} + T_{DS} - T_{SD}$$

$$A\,\frac{\partial h_B}{\partial t} = T_{DB} - T_{BD} - T_{BS}$$

where (h_S, h_D, h_B) represents the thickness of the surface (S), deep (D), and bottom (B) water layers respectively and A is the ocean area. The volume transports (or transformation rates) from layer i to j are represented as T_{ij} as shown in Figure 1b. (Note that it is assumed, for mathematical convenience, that upwelling in the Southern Ocean (T_{DB}) passes into the densest layer before transiting north via Ekman transport (T_{BS}).) We will diagnose the rate of transformation from the surface to deep layer T_{SD} (representing North Atlantic Deep Water formation) and T_{BD} (representing southern origin water formation and ventilation) at equilibrium. The deep layer depth can be calculated by an integral volume constraint,

$$D = h_S + h_D + h_B$$

where D is the total ocean depth.

The conservation of density is simplified by the definition of buoyancy,

$$b_i = \frac{-g(\rho_i - \rho_0)}{\rho_0}$$

where ρ_i is the layer density, ρ_0 a constant reference density, and g the acceleration due to gravity. Equations for the surface and bottom layers respectively are

$$A\,h_S\frac{\partial b_S}{\partial t} = -A\,b_S\frac{\partial h_S}{\partial t} + Q_S + b_D\,T_{DS} - q_{SD} - b_S\,T_{SD} + b_B\,T_{BS}$$

$$A\,h_B\frac{\partial b_B}{\partial t} = -A\,b_B\,\frac{\partial h_B}{\partial t} - Q_B - b_B\,T_{BS} + b_D\,T_{DB} - b_B\,T_{BD} + q_{DB}$$

where Q_i represents the flux of buoyancy into the layer at the surface (which, for the deep and bottom layers, acts to increase density over layer outcrop regions) and q_{ij} is the downward vertical diffusive flux of buoyancy. The deep layer is closed by the global conservation equation

$$Db_0 = h_S b_S + h_D b_D + h_B b_B$$

where b_0 is the mean buoyancy. Note that we have assumed that T_{BS} is positive.

Following *Shakespeare and Hogg* [2012], we parameterize each of the water mass transformations from existing theory. Northward transport into the surface layer in the Southern Ocean region is a combination of wind-driven (Ekman) transport, compensated by southward eddy fluxes,

$$T_{BS} = T_{\mathrm{Ek}} - T_{e,S} = \frac{\tau L_x}{\rho_0 f_{\mathrm{ACC}}} - a_{e,S}\,\Delta b_{SB}\,h_S^2$$

where eddy fluxes are parameterized with a prescribed coefficient described by the parameter $a_{e,S}$ and $\Delta b_{SB} = b_S - b_b$ [*Visbeck et al.*, 1997]. Transport out of the deep layer in the Southern Ocean region is entirely due to eddy fluxes,

$$T_{DB} = T_{e,D} = a_{e,D}\,\Delta b_{DB}\,h_D^2$$

while conversion of surface to deep water in the northern regions is calculated as per *de Boer et al.* [2010a]

$$T_{SD} = a_{SD}\,\Delta b_{SD}\,h_S^2.$$

We assume a form for the diffusive fluxes at each of the interfaces by approximating the vertical density gradient as follows:

$$q_{SD} = -2K_v A\,\frac{b_S - b_D}{h_S + h_D}$$

$$q_{DB} = -K_v A\,\frac{b_D - b_B}{h_D}$$

where K_v is a prescribed vertical eddy diffusivity, with a local balance between vertical transport and diffusive flux giving

$$T_{DS} = \frac{2K_v A}{h_S + h_D} = \frac{-q_{SD}}{b_S - b_D}$$

$$T_{BD} = \frac{K_v A}{h_D} = \frac{-q_{DB}}{b_D - b_B}.$$

A key component of this model is that we allow K_v to vary in the vertical so that the elevation of each interface will control the effective diffusivity of buoyancy through that interface. The specific parameter choices are outlined in Table 1.

Acknowledgments
The Smith and Sandwell topography data are available online at NASA page http://gcmd.nasa.gov/records/GCMD_SIO_NOAA_SEAFLOORTOPO.html. The data set title is Measured and Estimated Seafloor Topography. This work was undertaken while A.M.H. was on sabbatical leave, hosted by Atmospheric, Oceanic and Planetary Physics, Department of Physics, University of Oxford. A.M.H. was supported by Australian Research Council Future Fellowship FT120100842. Our thanks to M. Nikurashin, R. Toggweiler, and D. Sigman who provided comments on an early draft of this manuscript.

The Editor thanks two anonymous reviewers for their assistance in evaluating this paper.

References

Adkins, J. F. (2013), The role of deep ocean circulation in setting glacial climates, *Paleoceanography*, *28*, 539–561, doi:10.1002/palo.20046.
Bouttes, N., D. Paillard, and D. M. Roche (2010), Impact of brine-induced stratification on the glacial carbon cycle, *Clim. Past*, *6*(5), 575–589, doi:10.5194/cp-6-575-2010.
Bouttes, N., D. Paillard, D. M. Roche, V. Brovkin, and L. Bopp (2011), Last Glacial Maximum CO_2 and $\delta^{13}C$ successfully reconciled, *Geophys. Res. Lett.*, *38*, L02705, doi:10.1029/2010GL044499.
Bryan, K., and L. J. Lewis (1979), A water mass model of the world ocean, *J. Geophys. Res.*, *84*(C5), 2503–2517, doi:10.1029/JC084iC05p02503.
Burke, A., and L. F. Robinson (2012), The Southern Ocean's role in carbon exchange during the last deglaciation, *Science*, *335*(6068), 557–561, doi:10.1126/science.1208163.
Curry, W. B., and D. W. Oppo (2005), Glacial water mass geometry and the distribution of $\delta^{13}C$ of ΣCO2 in the western Atlantic Ocean, *Paleoceanography*, *20*, PA1017, doi:10.1029/2004PA001021.
De Boer, A. M., D. M. Sigman, J. R. Toggweiler, and J. L. Russell (2007), The effect of global ocean temperature change on deep ocean ventilation, *Paleoceanography*, *22*, PA2210, doi:10.1029/2005PA001242.
De Boer, A. M., J. R. Toggweiler, and D. M. Sigman (2008), Atlantic dominance of the meridional overturning circulation, *J. Phys. Oceanogr.*, *38*(2), 435–450, doi:10.1175/2007JPO3731.1.
De Boer, A. M., A. Gnanadesikan, N. R. Edwards, and A. J. Watson (2010a), Meridional density gradients do not control the Atlantic overturning circulation, *J. Phys. Oceanogr.*, *40*(2), 368–380, doi:10.1175/2009JPO4200.1.
De Boer, A. M., A. J. Watson, N. R. Edwards, and K. I. C. Oliver (2010b), A multi-variable box model approach to the soft tissue carbon pump, *Clim. Past*, *6*(6), 827–841, doi:10.5194/cp-6-827-2010.
Dewar, W. K., and A. M. Hogg (2010), Topographic inviscid dissipation of balanced flow, *Ocean Modell.*, *32*(1–2), 1–13, doi:10.1016/j.ocemod.2009.03.007.
Gnanadesikan, A. (1999), A simple predictive model for the structure of the oceanic pycnocline, *Science*, *283*, 2077–2079.
Hodell, D. A., K. A. Venz, C. D. Charles, and U. S. Ninnemann (2003), Pleistocene vertical carbon isotope and carbonate gradients in the South Atlantic sector of the Southern Ocean, *Geochem. Geophys. Geosyst.*, *4*(1), 1004, doi:10.1029/2002GC000367.
Ito, T., and M. J. Follows (2005), Preformed phosphate, soft tissue pump and atmospheric CO_2, *J. Mar. Res.*, *63*(4), 813–839.
Kamenkovich, I. V., and P. J. Goodman (2000), The dependence of AABW transport in the Atlantic on vertical diffusivity, *Geophys. Res. Lett.*, *27*(22), 3739–3742, doi:10.1029/2000GL011675.
Ledwell, J. R., E. T. Montgomery, K. L. Polzin, L. S. Laurent, R. W. Schmitt, and J. M. Toole (2000), Evidence for enhanced mixing over rough topography in the abyssal ocean, *Nature*, *403*(6766), 179–182.
Lund, D. C., J. F. Adkins, and R. Ferrari (2011), Abyssal Atlantic circulation during the Last Glacial Maximum: Constraining the ratio between transport and vertical mixing, *Paleoceanography*, *26*, PA1213, doi:10.1029/2010PA001938.
Lynch Stieglitz, J., A. Geen, and R. G. Fairbanks (1996), Interocean exchange of glacial North Atlantic Intermediate Water: Evidence from subantarctic Cd/Ca and carbon isotope measurements, *Paleoceanography*, *11*(2), 191–201, doi:10.1029/95PA03772.
Mellor, G. L., and T. Yamada (1982), Development of a turbulence closure model for geophysical fluid problems, *Rev. Geophys.*, *20*(4), 851–875, doi:10.1029/RG020i004p00851.
Nikurashin, M., and R. Ferrari (2010), Radiation and dissipation of internal waves generated by geostrophic motions impinging on small-scale topography: Theory, *J. Phys. Oceanogr.*, *40*(5), 1055–1074, doi:10.1175/2009JPO4199.1.
Nikurashin, M., and R. Ferrari (2013), Overturning circulation driven by breaking internal waves in the deep ocean, *Geophys. Res. Lett.*, *40*, 3133–3137, doi:10.1002/grl.50542.
Otto-Bliesner, B. L., C. D. Hewitt, T. M. Marchitto, E. Brady, A. Abe-Ouchi, M. Crucifix, S. Murakami, and S. L. Weber (2007), Last Glacial Maximum ocean thermohaline circulation: PMIP2 model intercomparisons and data constraints, *Geophys. Res. Lett.*, *34*, L12706, doi:10.1029/2007GL029475.
Polzin, K. L., J. M. Toole, J. R. Ledwell, and R. W. Schmitt (1997), Spatial variability of turbulent mixing in the abyssal ocean, *Science*, *276*(5309), 93–96.
Saenko, O. A., X. Zhai, W. J. Merryfield, and W. G. Lee (2012), The combined effect of tidally and eddy-driven diapycnal mixing on the large-scale ocean circulation, *J. Phys. Oceanogr.*, *42*(4), 526–538, doi:10.1175/JPO-D-11-0122.1.
Shakespeare, C. J., and A. M. Hogg (2012), An analytical model of the response of the meridional overturning circulation to changes in wind and buoyancy forcing, *J. Phys. Oceanogr.*, *42*, 1270–1287, doi:10.1175/JPO-D-11-0198.1.
Sigman, D. M., and E. A. Boyle (2000), Glacial/interglacial variations in atmospheric carbon dioxide, *Nature*, *407*(6806), 859–869.
Sigman, D. M., M. P. Hain, and G. H. Haug (2010), The polar ocean and glacial cycles in atmospheric CO, *Nature*, *466*(7302), 47–55, doi:10.1038/nature09149.
Skinner, L. C. (2009), Glacial-interglacial atmospheric CO_2 change: A possible"standing volume" effect on deep-ocean carbon sequestration, *Clim. Past*, *5*(3), 537–550.
Smith, W. H. F., and D. T. Sandwell (1997), Global seafloor topography from satellite altimetry and ship depth soundings, *Science*, *277*, 1956–1962.

Toggweiler, J. R., J. L. Russell, and S. R. Carson (2006), Midlatitude westerlies, atmospheric CO_2, and climate change during the ice ages, *Paleoceanography*, *21*, PA2005, doi:10.1029/2005PA001154.

Visbeck, M., J. Marshall, T. Haine, and M. Spall (1997), Specification of eddy transfer coefficients in coarse-resolution ocean circulation models, *J. Phys. Oceanogr.*, *27*, 381–402.

Watson, A. J., and A. C. N. Garabato (2006), The role of Southern Ocean mixing and upwelling in glacial-interglacial atmospheric CO_2 change, *Tellus*, *58B*, 73–87.

Weber, S. L., S. S. Drijfhout, A. Abe-Ouchi, M. Crucifix, M. Eby, A. Ganopolski, S. Murakami, B. Otto-Bliesner, and W. R. Peltier (2007), The modern and glacial overturning circulation in the Atlantic Ocean in PMIP coupled model simulations, *Clim. Past*, *3*(1), 51–64.

Zhai, X., H. L. Johnson, and D. P. Marshall (2010), Significant sink of ocean-eddy energy near western boundaries, *Nat. Geosci.*, *3*(9), 608–612, doi:10.1038/ngeo943.